

Majorana Fermion Dark Matter in Minimally Extended Left-Right Symmetric Model

M. J. Neves,^{1,2,*} Nobuchika Okada,^{1,†} and Satomi Okada^{1,‡}

¹*Department of Physics and Astronomy,
University of Alabama, Tuscaloosa, AL 35487, USA*

²*Departamento de Física, Universidade Federal Rural do Rio de Janeiro,
BR 465-07, 23890-971, Seropédica, RJ, Brazil*

Abstract

We present a minimal extension of the left-right symmetric model based on the gauge group $SU(3)_c \times SU(2)_L \times SU(2)_R \times U(1)_{B-L} \times U(1)_X$, in which a vector-like fermion pair (ζ_L and ζ_R) charged under the $U(1)_{B-L} \times U(1)_X$ symmetry is introduced. Associated with the symmetry breaking of the gauge group $SU(2)_R \times U(1)_{B-L} \times U(1)_X$ down to the Standard Model (SM) hypercharge $U(1)_Y$, Majorana masses for $\zeta_{L,R}$ are generated and the lightest mass eigenstate plays a role of the dark matter (DM) in our universe by its communication with the SM particles through a new neutral gauge boson “X”. We consider various phenomenological constraints of this DM scenario, such as the observed DM relic density, the LHC Run-2 constraints from the search for a narrow resonance, and the perturbativity of the gauge couplings below the Planck scale. Combining all constraints, we identify the allowed parameter region which turns out to be very narrow. A significant portion of the currently allowed parameter region will be tested by the High-Luminosity LHC experiments.

* mneves@ua.edu

† okadan@ua.edu

‡ satomi.okada@ua.edu

I. INTRODUCTION

The left-right symmetric model (LRSM) is one of well-motivated models beyond the Standard Model (SM), which was introduced for understanding the origin of the parity violation in the SM [1–3]. The model is based on the gauge group $SU(3)_c \times SU(2)_L \times SU(2)_R \times U(1)_{B-L}$. The leptonic $SU(2)_R$ doublet includes the right-handed neutrinos (RHNs), and the spontaneous symmetry breaking of $SU(2)_R \times U(1)_{B-L}$ to the SM $U(1)_Y$ generates Majorana masses for the RHNs. With the subsequent electroweak symmetry breaking, tiny SM neutrino masses are naturally generated by the type-I seesaw mechanism [4–8]. New charged and neutral gauge bosons, W_R and Z_R , predicted by the model have been searched for by the Large Hadron Collider (LHC) experiments [9–11].

Although the LRSM is very interesting, a DM candidate is missing in its minimal version. Simple extensions of the LRSM to incorporate a fermion or scalar DM candidate have been proposed in Refs. [12–14], and then their DM phenomenologies have been investigated in detail [15–18], where the DM interactions with the SM particles through W_R and Z_R play a central role. In another approach, the LRSM can be minimally extended to incorporate a new $U(1)_X$ gauge group and a Dirac fermion DM which is singlet under the SM gauge group [19] (see also Ref. [20]). In this scenario, the DM particle communicates with the SM particles through a massive gauge boson (X), which arises as a linear combination of the $SU(2)_R$, $U(1)_{B-L}$ and $U(1)_X$ gauge bosons after the symmetry breaking of $SU(2)_R \times U(1)_{B-L} \times U(1)_X$ down to the SM $U(1)_Y$. This class of DM models is called “ Z' -portal DM scenario” (for a review, see Ref. [21] and references therein).

In this paper, we consider a Majorana fermion DM in the context of a minimal extension of the LRSM with a new $U(1)_X$ gauge symmetry, which is based on the gauge group $SU(3)_c \times SU(2)_L \times SU(2)_R \times U(1)_{B-L} \times U(1)_X$. As mentioned above, this minimal $U(1)_X$ extension has been proposed in Ref. [19] to incorporate a Dirac fermion DM, where the $U(1)_X$ symmetry ensures the stability of the Dirac fermion and the DM fermion communicates with the SM particles through the massive gauge boson X . Although the gauge group and the particle content of our model is the same as those in Ref. [19], we consider in this paper a modification of the $U(1)_{B-L} \times U(1)_X$ charge assignment for the vector-like fermion pair (ζ_L and ζ_R) by which their Majorana masses are generated by the symmetry breaking, in addition to the Dirac mass. As a result, the lightest Majorana mass eigenstate plays a role

of the DM in our universe. We carefully calculate the gauge boson mass eigenstates after the symmetry breaking of $SU(2)_R \times U(1)_{B-L} \times U(1)_X$ down to the SM $U(1)_Y$ to derive the massive gauge boson X couplings with the DM fermion and the SM fermions. Errors in the coupling formulas presented in Ref. [19] will be corrected in this paper. We consider various phenomenologies of our DM scenario, such as the observed DM relic density, the LHC Run-2 constraints on the X boson and theoretical consistency, namely, the perturbativity condition on the gauge couplings up to the reduced Planck scale. Combining all the constraints, we identify the allowed parameter region, which turns out to be very narrow.

This paper is organized as follows: In Sec. II, we present the minimally extended LRSM with a Majorana fermion DM. In Sec. III, we discuss the symmetry breaking of the model down to the SM gauge group and derive the gauge boson mass spectrum. We also derive the gauge boson interactions with the SM fermions and the DM particle. The perturbativity condition of the gauge coupling constants will be investigated in Sec. IV. In Sec. V, we consider the LHC Run-2 constraints on the X boson mass and its coupling with the SM fermions. We will see that the allowed mass range of the X boson is very restricted after combining the LHC Run-2 constraints and the perturbativity condition. In Sec. VI, we analyze the relic density of the Majorana fermion DM and identify the model parameter region to reproduce the observed DM relic density. We combine all the constraints to see the allowed parameter region. The last section is devoted to conclusions.

II. MINIMALLY EXTENDED LRSM WITH MAJORANA FERMION DM

As has been first proposed in Ref. [19], the minimally extended LRSM is based on the gauge group $\mathcal{G}_{LRX} \equiv SU(3)_c \times SU(2)_L \times SU(2)_R \times U(1)_{B-L} \times U(1)_X$. The introduction of the new gauge symmetry $U(1)_X$ is the key of the extension. The particle content of the model is listed in Table I. Along with the $U(1)_X$ gauge symmetry, a new scalar ϕ_X and a vector-like pair of the fermions $\zeta_{L,R}$ are introduced. All fields in the original LRSM are singlet under the $U(1)_X$. Note that the charge assignment for $\zeta_{L,R} : (-a/2, a/2)$ is crucial to generate Majorana mass terms for $\zeta_{L,R}$, while $(-b/2, b/2)$ with $b \neq a$ is assigned in Ref. [19].

The kinetic terms for the fermions are expressed as

$$\mathcal{L}_f = \overline{\psi}_L^i i\gamma^\mu D_\mu \psi_L^i + \overline{\psi}_R^i i\gamma^\mu D_\mu \psi_R^i + \overline{Q}_L^i i\gamma^\mu D_\mu Q_L^i + \overline{Q}_R^i i\gamma^\mu D_\mu Q_R^i + \overline{\zeta}_L i\gamma^\mu D_\mu \zeta_L + \overline{\zeta}_R i\gamma^\mu D_\mu \zeta_R, \quad (1)$$

| | $SU(3)_c$ | $SU(2)_L$ | $SU(2)_R$ | $U(1)_{B-L}$ | $U(1)_X$ |
|---|--------------------------|--------------------------|--------------------------|--------------|----------|
| $Q_L^i = \begin{pmatrix} u_L^i \\ d_L^i \end{pmatrix}$ | $\underline{\mathbf{3}}$ | $\underline{\mathbf{2}}$ | $\underline{\mathbf{1}}$ | +1/3 | 0 |
| $Q_R^i = \begin{pmatrix} u_R^i \\ d_R^i \end{pmatrix}$ | $\underline{\mathbf{3}}$ | $\underline{\mathbf{1}}$ | $\underline{\mathbf{2}}$ | +1/3 | 0 |
| $\Psi_L^i = \begin{pmatrix} \nu_L^i \\ e_L^i \end{pmatrix}$ | $\underline{\mathbf{1}}$ | $\underline{\mathbf{2}}$ | $\underline{\mathbf{1}}$ | -1 | 0 |
| $\Psi_R^i = \begin{pmatrix} N_R^i \\ e_R^i \end{pmatrix}$ | $\underline{\mathbf{1}}$ | $\underline{\mathbf{1}}$ | $\underline{\mathbf{2}}$ | -1 | 0 |
| Φ | $\underline{\mathbf{1}}$ | $\underline{\mathbf{2}}$ | $\underline{\mathbf{2}}$ | 0 | 0 |
| Δ_L | $\underline{\mathbf{1}}$ | $\underline{\mathbf{3}}$ | $\underline{\mathbf{1}}$ | +2 | 0 |
| Δ_R | $\underline{\mathbf{1}}$ | $\underline{\mathbf{1}}$ | $\underline{\mathbf{3}}$ | +2 | 0 |
| ϕ_X | $\underline{\mathbf{1}}$ | $\underline{\mathbf{1}}$ | $\underline{\mathbf{1}}$ | +a | -a |
| $\zeta_{L,R}$ | $\underline{\mathbf{1}}$ | $\underline{\mathbf{1}}$ | $\underline{\mathbf{1}}$ | -a/2 | +a/2 |

TABLE I. The particle content of our minimally extended LRSM with Majorana fermion DM. Along with the $U(1)_X$ gauge symmetry, a new scalar ϕ_X and a vector-like pair of the fermions $\zeta_{L,R}$ are introduced. All fields in the original LRSM are singlet under the $U(1)_X$. $i = 1, 2, 3$ is the generation index, and $a \neq 0$ is a real parameter.

where the covariant derivative D_μ (relevant for $SU(2)_L \times SU(2)_R \times U(1)_{B-L} \times U(1)_X$) is given by

$$D_\mu = \partial_\mu + ig_L A_{L\mu}^a \frac{\sigma_L^a}{2} + ig_R A_{R\mu}^a \frac{\sigma_R^a}{2} + ig_{BL} \frac{Q_{BL}}{2} B_\mu + ig_X \frac{Q_X}{2} C_\mu, \quad (2)$$

with corresponding gauge couplings, g_L , g_R , g_{BL} and g_X , and gauge bosons, $A_{L\mu}^a$, $A_{R\mu}^a$, B_μ , and C_μ . We impose the left-right parity symmetry, so that $g_L = g_R \equiv g$. The most general gauge bosons kinetic terms are given by

$$\mathcal{L}_{gauge} = -\frac{1}{2} \text{tr} (F_{L\mu\nu}^2) - \frac{1}{2} \text{tr} (F_{R\mu\nu}^2) - \frac{1}{4} B_{\mu\nu}^2 - \frac{1}{4} C_{\mu\nu}^2 - \frac{1}{2} \chi_{mix} B_{\mu\nu} C^{\mu\nu}, \quad (3)$$

where $F_{L\mu\nu}$, $F_{R\mu\nu}$, $B_{\mu\nu}$ and $C_{\mu\nu}$ are the field-strength tensors of $A_{L\mu}^a$, $A_{R\mu}^a$, B_μ , and C_μ , respectively. Although the general Lagrangian includes a kinetic mixing between $B_{\mu\nu}$ and $C_{\mu\nu}$, we set the mixing parameter $\chi_{mix} = 0$ through out this paper, for simplicity.

In the minimal LRSM, the Higgs potential for Φ and $\Delta_{L,R}$ and the symmetry breaking have been investigated in detail [22–30]. We extend the Higgs potential by adding ϕ_X as follows:

$$\begin{aligned}
V(\Phi, \Delta_{L,R}, \phi_X) = & -\mu_1^2 \text{Tr}(\Phi^\dagger \Phi) - \mu_2^2 \left[\text{Tr}(\tilde{\Phi} \Phi^\dagger) + \text{Tr}(\tilde{\Phi}^\dagger \Phi) \right] - \mu_3^2 \text{Tr}(\Delta_R \Delta_R^\dagger) \\
& + \lambda_1 [\text{Tr}(\Phi^\dagger \Phi)]^2 + \lambda_2 \left\{ [\text{Tr}(\tilde{\Phi} \Phi^\dagger)]^2 + [\text{Tr}(\tilde{\Phi}^\dagger \Phi)]^2 \right\} \\
& + \lambda_3 \text{Tr}(\tilde{\Phi} \Phi^\dagger) \text{Tr}(\tilde{\Phi}^\dagger \Phi) + \lambda_4 \text{Tr}(\Phi^\dagger \Phi) \left[\text{Tr}(\tilde{\Phi} \Phi^\dagger) + \text{Tr}(\tilde{\Phi}^\dagger \Phi) \right] \\
& + \rho_1 \left[\text{Tr}(\Delta_R \Delta_R^\dagger) \right]^2 + \rho_2 \text{Tr}(\Delta_R \Delta_R) \text{Tr}(\Delta_R^\dagger \Delta_R^\dagger) \\
& + \alpha_1 \text{Tr}(\Phi^\dagger \Phi) \text{Tr}(\Delta_R \Delta_R^\dagger) + \left[\alpha_2 e^{i\delta_2} \text{Tr}(\tilde{\Phi}^\dagger \Phi) \text{Tr}(\Delta_R \Delta_R^\dagger) + \text{H.c.} \right] \\
& + \alpha_3 \text{Tr}(\Phi^\dagger \Phi \Delta_R \Delta_R^\dagger) - \mu'^2 \phi_X^\dagger \phi_X + \lambda' \left(\phi_X^\dagger \phi_X \right)^2 \\
& + \eta_1 \left(\phi_X^\dagger \phi_X \right) \left[\text{Tr} \left(\Delta_L^\dagger \Delta_L \right) \right] + \eta_2 \left(\phi_X^\dagger \phi_X \right) \left[\text{Tr} \left(\Phi^\dagger \Phi \right) \right] + L \leftrightarrow R, \quad (4)
\end{aligned}$$

where μ_i ($i = 1, 2, 3$), μ' , λ_i ($i = 1, 2, 3, 4$), λ' , ρ_i ($i = 1, 2$), α_i ($i = 1, 2, 3$) and η_i ($i = 1, 2$) are real parameters. The electric charge operator in our model is given by

$$Q_{em} = I_{3L} + I_{3R} + \frac{Q_{BL}}{2} + \frac{Q_X}{2}, \quad (5)$$

where I_{3L} (I_{3R}) is the diagonal generators of $SU(2)_L$ ($SU(2)_R$), and Q_{BL} (Q_X) is a $U(1)_{B-L}$ ($U(1)_X$) charge. We may express the Higgs fields as

$$\Phi = \begin{pmatrix} \phi_1^0 & \phi_2^+ \\ \phi_1^- & \phi_2^0 \end{pmatrix}, \quad \Delta_L = \begin{pmatrix} \Delta_L^+/\sqrt{2} & \Delta_L^{++} \\ \Delta_L^0 & -\Delta_L^+/\sqrt{2} \end{pmatrix}, \quad \Delta_R = \begin{pmatrix} \Delta_R^+/\sqrt{2} & \Delta_R^{++} \\ \Delta_R^0 & -\Delta_R^+/\sqrt{2} \end{pmatrix}. \quad (6)$$

The gauge symmetry \mathcal{G}_{LRX} is broken down to $SU(3)_c \times U(1)_{em}$ by the following vacuum expectation values (VEVs):

$$\langle \Phi \rangle = \begin{pmatrix} \frac{v_1}{\sqrt{2}} & 0 \\ 0 & \frac{v_2}{\sqrt{2}} \end{pmatrix}, \quad \langle \Delta_L \rangle = \begin{pmatrix} 0 & 0 \\ \frac{v_L}{\sqrt{2}} & 0 \end{pmatrix}, \quad \langle \Delta_R \rangle = \begin{pmatrix} 0 & 0 \\ \frac{v_R}{\sqrt{2}} & 0 \end{pmatrix}, \quad \langle \phi_X \rangle = \frac{v_X}{\sqrt{2}}. \quad (7)$$

For simplicity, we choose the hierarchy among VEVs such that $v_L \ll \sqrt{v_1^2 + v_2^2} \ll v_X \ll v_R$, with $v_1 = v \sin \beta$, $v_2 = v \cos \beta$ and $v = 246$ GeV. The sequence of the gauge symmetry breaking is as follows: First, the $SU(2)_R \times U(1)_{B-L}$ symmetry is broken by v_R , yielding large masses for W_R and Z_R . Next, the $U(1)_X$ symmetry is broken by v_X and the mass of $U(1)_X$ gauge boson is generated. The electroweak symmetry breaking down to $U(1)_{em}$ is

completed by v_1 and v_2 . In the next section, we show the mass eigenvalues and corresponding eigenstates in detail.

The Yukawa couplings of the model are given by

$$\begin{aligned}
-\mathcal{L}_Y = & h_{ij}^{(\ell)} \overline{\psi}_L^i \Phi \psi_R^j + \tilde{h}_{ij}^{(\ell)} \overline{\psi}_L^i \tilde{\Phi} \psi_R^j + h_{ij}^{(Q)} \overline{Q}_L^i \Phi Q_R^j + \tilde{h}_{ij}^{(Q)} \overline{Q}_L^i \tilde{\Phi} Q_R^j \\
& + \frac{1}{2} f_{ij}^\psi \overline{\psi}_L^{i,c} \tilde{\Delta}_L \psi_L^j + \frac{1}{2} f_{ij}^\psi \overline{\psi}_R^{i,c} \tilde{\Delta}_R \psi_R^j + \frac{1}{2} Y^\zeta \phi_X \overline{\zeta}_L^c \zeta_L + \frac{1}{2} Y^\zeta \phi_X \overline{\zeta}_R^c \zeta_R + \text{H.c.}, \quad (8)
\end{aligned}$$

where $\tilde{\Phi} = \sigma_2 \Phi^* \sigma_2$, and $\tilde{\Delta}_{L(R)} = i \sigma_2 \Delta_{L(R)}$. Since we impose the parity symmetry, $\psi_L^i \leftrightarrow \psi_R^i$, $Q_L^i \leftrightarrow Q_R^i$, $\Delta_L \leftrightarrow \Delta_R$, $\Phi \leftrightarrow \Phi^\dagger$ and $\zeta_L \leftrightarrow \zeta_R$, the Yukawa matrices, $h_{ij}^{(\ell)}$, $\tilde{h}_{ij}^{(\ell)}$, $h_{ij}^{(Q)}$ and $\tilde{h}_{ij}^{(Q)}$, are Hermitian matrices. The Dirac mass matrices for leptons and quarks are generated by $\langle \Phi \rangle \neq 0$ while Majorana mass matrices for left and right-handed neutrinos are generated by $\langle \Delta_{L,R} \rangle \neq 0$, respectively. A common Majorana mass of $m = Y^\zeta v_X / \sqrt{2}$ for $\zeta_{L,R}$ is generated by $\langle \phi_X \rangle = v_X / \sqrt{2}$. Along with a gauge invariant Dirac mass term for $\zeta_{L,R}$ (M), the mass terms for ζ is given by

$$\mathcal{L}_{mass} = -\frac{1}{2} \begin{pmatrix} \overline{\zeta}_L^c & \overline{\zeta}_R \end{pmatrix} \begin{pmatrix} m & M \\ M & m \end{pmatrix} \begin{pmatrix} \zeta_L \\ \zeta_R^c \end{pmatrix} + \text{H.c.}, \quad (9)$$

where we set $M > m > 0$. The mass eigenvalues are given by $M_\pm = M \pm m$ and corresponding eigenstates, ζ_ℓ and ζ_h , are defined as $P_L \zeta_\ell = \frac{1}{\sqrt{2}} (\zeta_L - \zeta_R^c)$ and $P_L \zeta_h = \frac{1}{\sqrt{2}} (\zeta_L + \zeta_R^c)$, P_L is the left-hand projection operator. Thanks to the $U(1)_X$ symmetry, the lighter mass eigenstate ζ_ℓ is stable and identified with the Majorana fermion DM. In the following, we call the mass of DM ζ_ℓ as $m_{DM} \equiv M_- = M - m$.

III. MASS SPECTRUM AND EIGENSTATES OF THE GAUGE BOSONS

Through the gauge symmetry breaking by Higgs VEVs, the charged gauge bosons W_L and W_R in the LRSM acquire their masses as

$$M_{W_L} \simeq \frac{1}{2} g v \quad \text{and} \quad M_{W_R} \simeq \frac{1}{\sqrt{2}} g v_R. \quad (10)$$

Here, we have used the hierarchy $v \ll v_R$. The mass eigenstate W_L is identified with the SM W boson.

Since we have four neutral gauge bosons, $A_{3L\mu}$, $A_{3R\mu}$, B_μ and C_μ , and they mix with each other after the symmetry breaking, the analysis for their mass spectrum and eigenstates is complicated. According to the hierarchy, $v_L \ll v \ll v_X \ll v_R$, we focus on the neutral gauge

boson mass terms generated by the symmetry breaking of $SU(2)_R \times U(1)_{B-L} \times U(1)_X \rightarrow U(1)_Y$:

$$\mathcal{L}_{mass} = \frac{1}{2} \eta^{\mu\nu} (V_\mu)^T M_{sq} V_\nu, \quad (11)$$

where $V_\mu = (A_{3R\mu} \ B_\mu \ C_\mu)^T$, and the mass-squared matrix is given by

$$M_{sq} = \begin{pmatrix} g^2 v_R^2 & -g g_{BL} v_R^2 & 0 \\ -g g_{BL} v_R^2 & g_{BL}^2 v_R^2 + a^2 g_{BL}^2 v_X^2 & -a^2 g_{BL} g_X v_X^2 \\ 0 & -a^2 g_{BL} g_X v_X^2 & a^2 g_X^2 v_X^2 \end{pmatrix}. \quad (12)$$

We now diagonalize the mass matrix M_{sq} by a 3×3 orthogonal matrix \mathcal{R} such that

$$\mathcal{L}_{mass} = \frac{1}{2} \eta^{\mu\nu} (\tilde{V}_\mu)^T D_{sq} \tilde{V}_\nu, \quad (13)$$

where the mass eigenstates are defied as $\tilde{V}_\mu = (Y_\mu \ X_\mu \ Z_{R\mu})^T = \mathcal{R}^T V_\mu$, and $D_{sq} = \text{diag}(0, M_X^2, M_{Z_R}^2)$ is the mass eigenvalue matrix with

$$M_X \simeq |a| v_X \sqrt{g_X^2 + \frac{g^2 g_{BL}^2}{g^2 + g_{BL}^2}} \quad \text{and} \quad M_{Z_R} \simeq v_R \sqrt{g^2 + g_{BL}^2}. \quad (14)$$

Here, we have used $v_X \ll v_R$.¹ The massless state is identified with the SM hyper-charge gauge boson Y_μ , while $Z_{R\mu}$ is the heavy neutral boson in the LRSM. To determine the couplings of the gauge boson mass eigenstates with the SM fermions and the Majorana fermion DM, we need to find the form of \mathcal{R} . Since we set $\epsilon \equiv (v_X/v_R)^2 \ll 1$, for this purpose it is sufficient to give the form of the orthogonal matrix up to $\mathcal{O}(\epsilon)$:

$$\mathcal{R} = \begin{pmatrix} \frac{g_{BL} g_X}{\sqrt{g^2 g_{BL}^2 + g^2 g_X^2 + g_{BL}^2 g_X^2}} & -\frac{g(g_{BL}^2 + g_X^2)}{\sqrt{g_{BL}^2 + g_X^2} \sqrt{g^2 g_{BL}^2 + g^2 g_X^2 + g_{BL}^2 g_X^2}} & 0 \\ \frac{g g_X}{\sqrt{g^2 g_{BL}^2 + g^2 g_X^2 + g_{BL}^2 g_X^2}} & \frac{g_{BL} g_X^2}{\sqrt{g_{BL}^2 + g_X^2} \sqrt{g^2 g_{BL}^2 + g^2 g_X^2 + g_{BL}^2 g_X^2}} & -\frac{g_{BL}}{\sqrt{g_{BL}^2 + g_X^2}} \\ \frac{g g_{BL}}{\sqrt{g^2 g_{BL}^2 + g^2 g_X^2 + g_{BL}^2 g_X^2}} & \frac{g_{BL}^2 g_X}{\sqrt{g_{BL}^2 + g_X^2} \sqrt{g^2 g_{BL}^2 + g^2 g_X^2 + g_{BL}^2 g_X^2}} & \frac{g_X}{\sqrt{g_{BL}^2 + g_X^2}} \end{pmatrix} + \mathcal{O}(\epsilon). \quad (15)$$

By using \mathcal{R} , we rewrite the original gauge interactions in terms of the mass eigenstates. It is easy to check that the hyper-charge of a field (Q_Y) is given by

$$Q_Y = I_{3R} + \frac{Q_{BL}}{2} + \frac{Q_X}{2}, \quad (16)$$

¹ Our results of the gauge boson mass spectrum and their couplings with the fermions remain the same as long as $g_{BL} v_R^2 \gg a^2 g_{BL} v_X^2, a^2 g_X v_X^2$, as expected from the form of M_{sq} .

and the SM $U(1)_Y$ gauge coupling (g_Y) is related to $g_R = g$, g_{BL} and g_X by

$$\frac{1}{g_Y^2} = \frac{1}{g^2} + \frac{1}{g_{BL}^2} + \frac{1}{g_X^2}. \quad (17)$$

Using the values of g and g_Y at the weak scale which are fixed by $\frac{g^2 g_Y^2}{g^2 + g_Y^2} = e^2 \simeq \frac{4\pi}{128}$ and $\frac{g_Y^2}{g^2 + g_Y^2} = \sin^2 \theta_W \simeq 0.23$, we find

$$g_X = \frac{0.428 g_{BL}}{\sqrt{(g_{BL})^2 - (0.428)^2}}, \quad (18)$$

and hence $g_{BL} > 0.428$ for $g_X < \infty$. In the next section, we consider the perturbativity condition for g_{BL} and g_X up to the Planck scale and find more severe constraints on g_{BL} and g_X .

In the following sections, we will investigate the DM physics. Since the DM particle communicates with the SM particle through the X -portal interaction, we present the explicit forms for the couplings of the X -boson with the SM fermions and the Majorana fermion DM. Using the original gauge couplings and the orthogonal matrix \mathcal{R} , we find the interaction terms of the form,

$$\mathcal{L}_{int} = - \left(Q_Y^{fL} g_f \bar{f}_L \gamma^\mu f_L + Q_Y^{fR} g_f \bar{f}_R \gamma^\mu f_R + g_\zeta \bar{\zeta}_\ell \gamma^\mu \gamma_5 \zeta_\ell \right) X_\mu, \quad (19)$$

where f_L and f_R denote the left-handed and right-handed SM fermions, respectively, listed in Table I, $Q_Y^{fL,R}$ are their hyper-charges, we have used the Dirac fermion expression for the Majorana DM ζ_ℓ , and

$$\begin{aligned} g_f &= \frac{g g_Y}{0.428} \frac{\sqrt{(g_{BL})^2 - (0.428)^2}}{\sqrt{g^2 + (g_{BL})^2}}, \\ g_\zeta &= \frac{a}{4} \frac{g}{g_Y} \frac{0.428 g_{BL}}{\sqrt{(g_{BL})^2 - (0.428)^2}} \frac{g_{BL}}{\sqrt{g^2 + (g_{BL})^2}}. \end{aligned} \quad (20)$$

The couplings, g_f and g_ζ , are determined as a function of g_{BL} . In the following analysis, we see that our results remain the same for $a \rightarrow -a$, and hence we only consider $a > 0$ without loss of generality.

IV. THE PERTURBATIVITY CONDITION ON THE GAUGE COUPLINGS

We have derived the relation between g_{BL} and g_X in Eq. (18) to reproduce the SM $U(1)_Y$ gauge coupling constant. To justify our analysis in the perturbative expansion of the model,

| a | $g_{BL} _{min}$ | $g_X _{max}$ | $g_f _{min}$ | $g_\zeta _{max}$ | a | $g_{BL} _{max}$ | $g_X _{min}$ | $g_f _{max}$ | $g_\zeta _{min}$ |
|-----|-----------------|--------------|--------------|------------------|-----|-----------------|--------------|--------------|------------------|
| 0.3 | 0.428 | 9.06 | 0.0141 | 0.680 | 0.3 | 0.738 | 0.525 | 0.331 | 0.0538 |
| 1 | 0.431 | 3.74 | 0.0342 | 0.941 | 1 | 0.727 | 0.530 | 0.326 | 0.179 |
| 2 | 0.439 | 1.94 | 0.0670 | 0.986 | 2 | 0.692 | 0.545 | 0.309 | 0.361 |
| 3 | 0.453 | 1.30 | 0.102 | 1.01 | 3 | 0.644 | 0.573 | 0.284 | 0.550 |
| 5 | 0.511 | 0.783 | 0.183 | 1.10 | 5 | 0.538 | 0.706 | 0.208 | 1.02 |

TABLE II. The minimum and maximum values of g_{BL} , g_X , g_f and g_ζ for various values of a .

we impose a theoretical consistency condition, namely, the perturbativity condition on the gauge couplings. Let us define the condition as

$$g_{BL}(M_P) \leq 4\pi, \quad \text{and} \quad g_X(M_P) \leq 4\pi, \quad (21)$$

for the running gauge couplings at the reduced Planck mass, $M_P = 2.43 \times 10^{18}$ GeV.

To evaluate the gauge coupling values at low energies, $\mu < M_P$, we employ the renormalization group (RG) equations at the one-loop level:

$$\mu \frac{dg_{BL}}{d\mu} = \beta_{BL}(g_{BL}), \quad \text{and} \quad \mu \frac{dg_X}{d\mu} = \beta_X(g_X). \quad (22)$$

With the particle content in Table I, the beta functions of β_{BL} and β_X are calculated to be

$$\beta_{BL} = \left(\frac{28 + a^2}{6} \right) \frac{g_{BL}^3}{16\pi^2}, \quad \text{and} \quad \beta_X = \left(\frac{a^2}{6} \right) \frac{g_X^3}{16\pi^2}. \quad (23)$$

Solving the RG equations, we find the maximum values of g_{BL} and g_X at v_R ,

$$g_{BL}|_{max} = \frac{4\pi}{\sqrt{1 + \left(\frac{28+a^2}{3} \right) \ln \left[\frac{M_P}{v_R} \right]}} \quad \text{and} \quad g_X|_{max} = \frac{4\pi}{\sqrt{1 + \frac{a^2}{3} \ln \left[\frac{M_P}{v_R} \right]}}. \quad (24)$$

In this paper, we set $v_R = 10^5$ GeV. Since the v_R value is not far from the electroweak scale, we approximate $g_Y(v_R) = g_Y(v)$. Note that the relation between g_{BL} and g_X of Eq. (18) indicates that the maximum value of $g_{BL}|_{max}$ ($g_X|_{max}$) corresponds to the minimum value of $g_X|_{min}$ ($g_{BL}|_{min}$). Similarly, from Eq. (20), $g_f|_{max}$ and $g_\zeta|_{min}$ ($g_f|_{min}$ and $g_\zeta|_{max}$) correspond to $g_{BL}|_{max}$ ($g_{BL}|_{min}$).

In Fig. 1, we show $g_{BL}|_{max,min}$ (left panel) and $g_X|_{max,min}$ (right panel) as a function of a . The value of a is restricted to be $0 < a \leq 5.28$ from the consistency, $g_{BL}|_{min} \leq g_{BL}|_{max}$. In Fig. 2, we plot $g_f|_{max,min}$ (left panel) and $g_\zeta|_{min,max}$ (right panel) as a function of a , corresponding to $g_{BL}|_{max,min}$ in the left panel of Fig. 1. For several a values, we list the maximum and minimum values of g_{BL} , g_X , g_f and g_ζ in Table II.

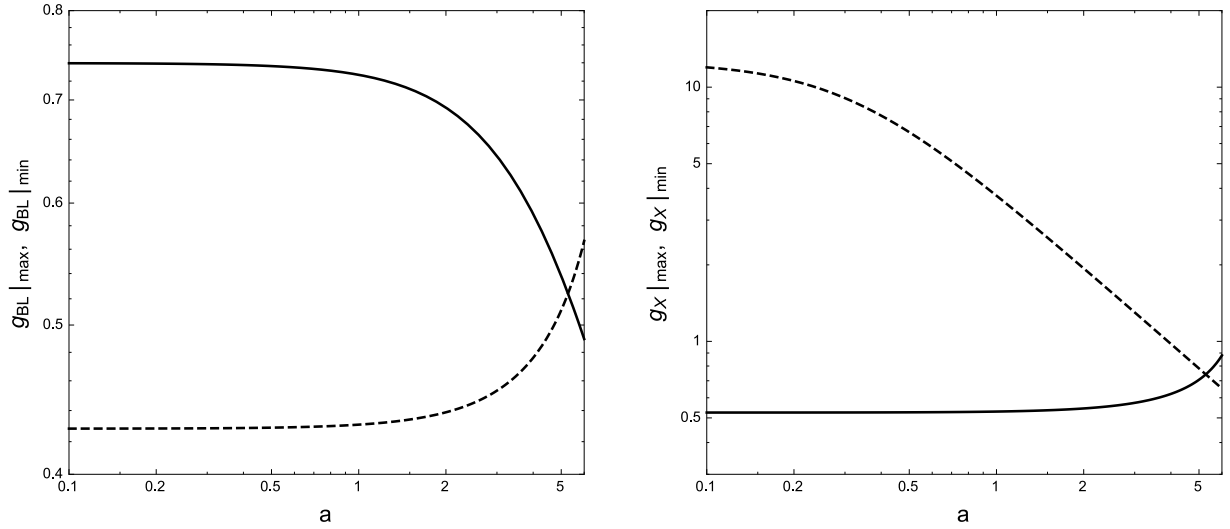


FIG. 1. *Left Panel:* The solid and dashed lines depict the maximum and minimum values of g_{BL} at $\mu = v_R = 10^5$ GeV, respectively, as a function of a . *Right Panel:* The minimum and maximum values of g_X as a function of a , which correspond to the maximum and minimum values of g_{BL} shown in Left Panel.

V. LHC CONSTRAINTS

In the gauge extension of the Standard Model, a new gauge boson appears. If kinematically allowed, such a gauge boson can be produced at many experiments, in particular, high energy collider experiments like the LHC experiment. The ATLAS and the CMS collaborations have been searching for a narrow resonance with a variety of final states, among which the results with dilepton final states provide the most severe constraints (unless the branching ratio of a resonance state is significantly suppressed). The ATLAS [31] and the CMS [32] collaborations have reported their final results with the full LHC Run-2 data, which very severely constrain the production cross section of a charge-neutral vector boson (so-called Z' boson). For example, let us consider the LHC search for the sequential SM Z' boson (Z'_{SSM}), whose interaction is exactly the same as that of the SM Z boson. Since no indication of Z'_{SSM} productions has been observed at the LHC Run-2, the lower bound on Z'_{SSM} boson mass has been obtained as $M_{Z'_{SSM}} \geq 5.1$ TeV by the ATLAS results [31] with 139/fb integrated luminosity and $M_{Z'_{SSM}} \geq 5.15$ TeV by the CMS results [32] with 140/fb integrated luminosity. Our model includes 3 new gauge bosons, namely, W_R , Z_R and X . Since we set $v_R = 10^5$ GeV $\gg v_X$, W_R and Z_R are too heavy to be produced at the LHC.

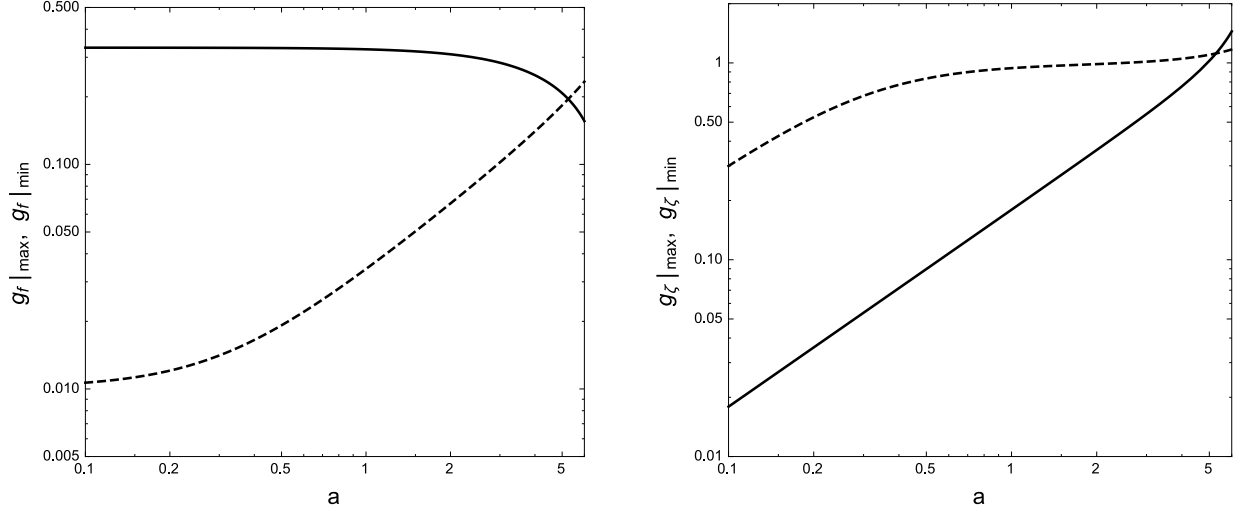


FIG. 2. *Left Panel:* The maximum (solid line) and minimum (dashed line) values of g_f as a function of a , corresponding to $g_{BL}|_{max}$ and $g_{BL}|_{min}$. *Right Panel:* The maximum (dashed line) and minimum (solid line) values of g_ζ as a function of a , corresponding to $g_{BL}|_{max}$ and $g_{BL}|_{min}$.

In this section, we consider the production of the X boson at the LHC and the current constraints on the X boson production by the narrow resonance search with dilepton final states.

We first calculate the X boson partial decay width into a pair of SM chiral fermions ($f_{L,R}$) (neglecting their masses) and a pair of DM particles ζ_ℓ :

$$\begin{aligned} \Gamma(X \rightarrow \overline{f_{L(R)}} f_{L(R)}) &= N_c \frac{g_f^2}{24\pi} (Q_Y^{f_{L(R)}})^2 M_X, \\ \Gamma(X \rightarrow \zeta_\ell \zeta_\ell) &= \frac{g_\zeta^2}{24\pi} M_X \left(1 - \frac{4m_{DM}^2}{M_X^2}\right)^{3/2}, \end{aligned} \quad (25)$$

where $N_c = 1(3)$ is the color factor for a SM lepton (quark), and we have assumed that the the X boson decay into ζ_h is kinematically forbidden, for simplicity. The total decay width of the X boson is the sum of partial widths to all SM fermions and the DM particles. As we will discuss in the next section, $m_{DM} \simeq M_X/2$ is required to reproduce the observed DM relic density, and the contribution of $\Gamma(X \rightarrow \zeta_\ell \zeta_\ell)$ to the total decay width is found to be negligibly small. Thus, we neglect $\Gamma(X \rightarrow \zeta_\ell \zeta_\ell)$ in our LHC analysis.

In evaluating the X boson production cross section at the LHC, we first notice that the LHC Run-2 constraints are very severe on Z' boson productions, so that we expect that the X boson coupling with the SM fermions is constrained to be $g_f \ll 1$. This means that the total X boson decay width (Γ_X) is very narrow, and we use the narrow width approximation

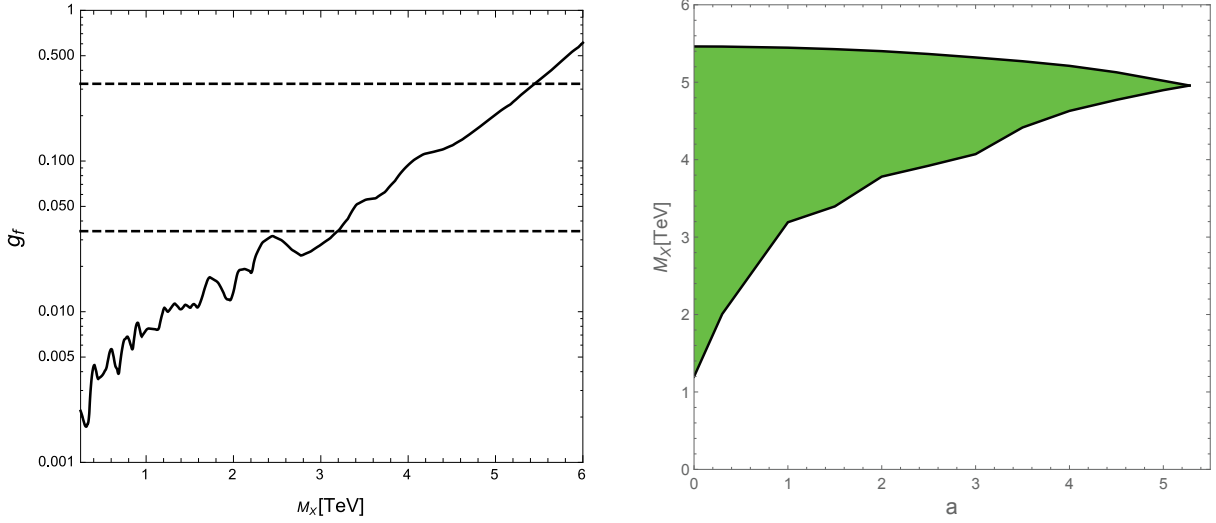


FIG. 3. *Left Panel:* The upper bound on g_f (solid line) as a function of M_X from the ATLAS results [31]. Along with the LHC bound, we also show the perturbativity condition on g_f . The two horizontal lines depict $g_f|_{min}$ and $g_f|_{max}$ for $a = 1$. Combining the LHC bound and the perturbativity condition, we find the allowed region, $3.19 \leq M_X[\text{TeV}] \leq 5.45$ for $a = 1$. *Right Panel:* The allowed region of M_X (green shaded) for various values of a after combining the LHC bound and the perturbativity condition.

in our calculation. In this approximation, the X boson production cross section at the parton level ($q\bar{q} \rightarrow X$) is given by

$$\hat{\sigma}(\hat{s}) = \frac{4\pi^2}{3} \frac{\Gamma(X \rightarrow q\bar{q})}{M_X} \delta(\hat{s} - M_X^2), \quad (26)$$

where \hat{s} is the invariant mass squared of the colliding partons (quarks). With this $\hat{\sigma}$, the cross section of the process $pp \rightarrow X$ at the LHC Run-2 with $\sqrt{s} = 13$ TeV is calculate by

$$\sigma(pp \rightarrow X) = 2 \sum_{q, \bar{q}} \int_0^1 dx \int_0^1 dy f_q(x, Q) f_{\bar{q}}(y, Q) \hat{\sigma}(xys), \quad (27)$$

where f_q ($f_{\bar{q}}$) is the parton distribution function (PDF) for a quark (anti-quark). For the PDFs, we employ CTEQ6L [33] with a factorization scale $Q = M_X$, for simplicity.

We obtain $\sigma(pp \rightarrow X) \text{BR}(X \rightarrow \ell^+ \ell^-)$ as a function of g_f and M_X . In the narrow decay width approximation, this cross section is proportional to g_f^2 . Comparing our cross section with the upper bound by the ATLAS collaboration [31] for fixed M_X values, we obtain the upper bound on g_f as a function of M_X . Our result is shown in Fig. 3. The left panel depicts the upper bound on g_f (solid line). We also show $g_f|_{min}$ and $g_f|_{max}$ for $a = 1$, as an example,

from the perturbativity condition discussed in the previous section. Combining the LHC bounds and perturbativity condition, we find the allowed region, $3.19 \leq M_X[\text{TeV}] \leq 5.45$ for $a = 1$. For various a values, we identify the allowed region of M_X , which is shown in the right panel of Fig. 3 (green shaded region).

VI. COSMOLOGICAL CONSTRAINT

The DM particle ζ_ℓ in our model can communicate with the SM particles through its interactions with the X and Z_R bosons and the Higgs bosons. For simplicity, we assume that the mixings of ϕ_X with Φ and $\Delta_{L,R}$ are very small and hence Higgs boson mediated interactions are unimportant for the DM physics. Since we have set $v_R = 10^5$ GeV and the Z_R boson is very heavy, the DM particle communicates with the SM particles mainly through its interaction with the X boson given in Eq. (19). In this section, we investigate this “ X -portal DM” scenario to identify the allowed parameter region from the cosmological constraint, namely, the observed DM relic density.

In the early universe, the DM particle ζ_ℓ was in thermal equilibrium with the SM particles through its X boson interaction. Due to the expansion of the universe, the DM particle decoupled from the SM particle thermal plasma at the freeze-out time in the early universe and then the total number of the DM particles in the universe is fixed. At the freeze-out time, we consider two main processes for the DM pair annihilations: (i) $\zeta_\ell \zeta_\ell \rightarrow X \rightarrow f_{SM} \overline{f_{SM}}$ and (ii) $\zeta_\ell \zeta_\ell \rightarrow X X$, where f_{SM} represents an SM fermion. The annihilation cross sections are controlled by four parameters: m_{DM} , M_X , g_f and g_ζ . With Eq. (20), we use m_{DM} , M_X , $g_{BL}(\mu = v_R)$ and a as free parameters in our DM physics analysis. As we have discussed in Secs. IV and V, once we fix a value for a , the range of g_{BL} is constrained by the perturbativity condition, and combining it with the LHC constraints, the range of M_X is also restricted. Note that for $m_{DM} \simeq M_X/2$, the process (i) dominates the annihilation cross section through X boson resonance effect. The process (ii) is relevant only for $m_{DM} > M_X$.

For evaluating the DM relic density, we solve the Boltzmann equation (for a review, see Refs. [35, 36]):

$$\frac{dY}{dx} = -\frac{s(m_{DM})}{H(m_{DM})} \frac{\langle \sigma v_{rel} \rangle}{x^2} (Y^2 - Y_{EQ}^2), \quad (28)$$

where the (photon) temperature of the universe (T) is normalized by $x = m_{DM}/T$, $s(m_{DM})$ and $H(m_{DM})$ are the entropy density and the Hubble parameter at $T = m_{DM}$, respectively,

Y is the yield of DM particle (the ratio of the DM number density to the entropy density), Y_{EQ} is the yield of the DM particle in thermal equilibrium, and $\langle\sigma v_{rel}\rangle$ is the thermal average of the DM annihilation cross section (σ) times relative velocity (v_{rel}). Explicit formulas of s , H and $Y_{EQ}(x)$ are given as follows:

$$\begin{aligned} s(T) &= \frac{2\pi^2}{45} g_* T^3 = \frac{2\pi^2}{45} g_* \left(\frac{m_{DM}}{x}\right)^3, \\ H(T) &= \sqrt{\frac{\pi^2}{90}} g_* \frac{T^2}{M_P}, \\ s Y_{EQ} &= \frac{g_{DM}}{2\pi^2} \left(\frac{m_{DM}}{x}\right)^3 x^2 K_2(x), \end{aligned} \quad (29)$$

where $g_{DM} = 2$ is the number of degrees of freedom for the Majorana fermion DM ζ_ℓ , g_* is the effective total number of degrees of freedom for the particles in thermal equilibrium (in our analysis, we use $g_* = 106.75$ for the SM particles), and K_2 is the modified Bessel function of the second kind. The thermal averaged annihilation cross section is given by

$$\langle\sigma v_{rel}\rangle = (s Y_{EQ})^{-2} g_{DM}^2 \frac{m_{DM}}{64\pi^4 x} \int_{(2m_{DM})^2}^{\infty} ds 2(s - (2m_{DM})^2) \sigma(s) \sqrt{s} K_1\left(\frac{x\sqrt{s}}{m_{DM}}\right), \quad (30)$$

where $\sigma(s)$ is the DM pair annihilation cross section, and K_1 is the modified Bessel function of the first kind. Solving the Boltzmann equation with the initial condition $Y(x) = Y_{EQ}(x)$ for $x \ll 1$, the DM relic density at present is evaluated by

$$\Omega_{DM} h^2 = \frac{m_{DM} s_0 Y(x_0)}{\rho_c/h^2}, \quad (31)$$

where $s_0 = 2890 \text{ cm}^3$ is the entropy density of the present universe, $\rho_c/h^2 = 1.05 \times 10^{-5} \text{ GeV/cm}^3$ is the critical density, and $Y(x_0)$ is the DM yield at present ($x_0 \gg 1$). We impose the cosmological constraint, namely, $\Omega_{DM} h^2 = 0.12$ to reproduce the observed DM relic density set by the Planck 2018 measurements [34].

We first consider the parameter region $m_{DM} \simeq M_X/2$, in which case the DM pair annihilation process (i) dominates the annihilation cross section by the X boson resonance effect. For the process $\zeta_\ell \zeta_\ell \rightarrow X \rightarrow f_{L(R)} \overline{f_{L(R)}}$, we find the annihilation cross section of the form:

$$\sigma(s) = \frac{g_\zeta^2 g_f^2}{48\pi} \frac{\sqrt{s(s - 4m_{DM}^2)}}{(s - M_X^2)^2 + M_X^2 \Gamma_X^2} \left(\sum_{f_L} N_c (Q_Y^{f_L})^2 + \sum_{f_R} N_c (Q_Y^{f_R})^2 \right), \quad (32)$$

where we have neglected the SM fermion masses since M_X is constrained to be in the range of $1 \lesssim M_X [\text{TeV}] \lesssim 5.5$ as discussed in the previous section (see the right panel of Fig. 3).

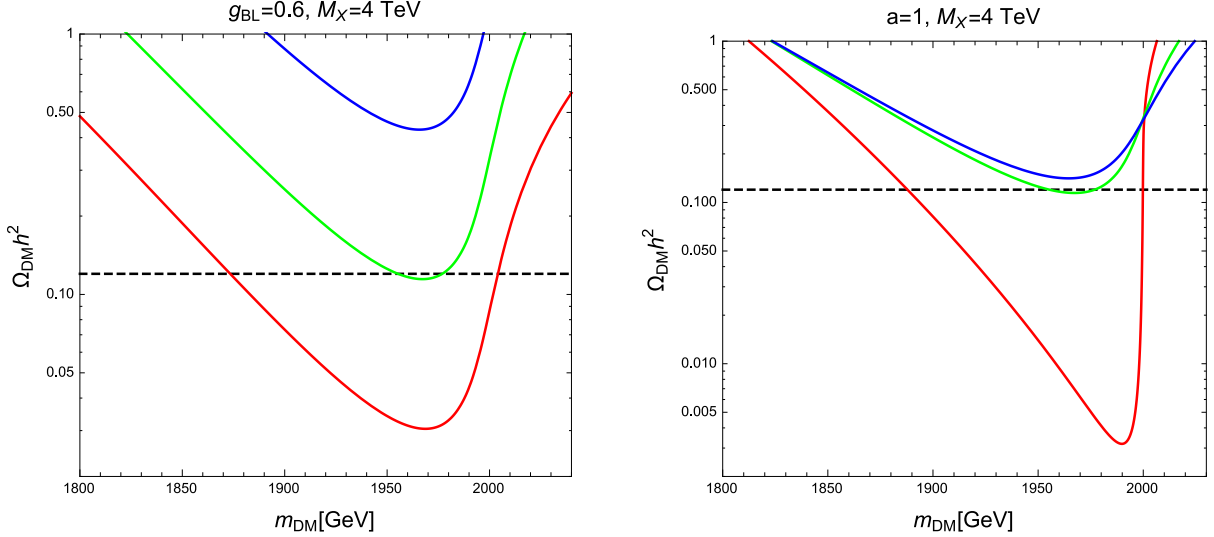


FIG. 4. *Left Panel:* The resultant DM relic densities for $a = 0.5$ (blue), $a = 1$ (green) and $a = 2$ (red), respectively, as a function of m_{DM} , along with the observed value (dashed horizontal line) of $\Omega_{DM}h^2 = 0.12$. In this analysis, we have fixed $g_{BL} = 0.6$ and $M_X = 4$ TeV. *Right Panel:* The resultant DM relic densities for $a = 1$ and $M_X = 4$ TeV, along with the observed value (dashed horizontal line) of $\Omega_{DM}h^2 = 0.12$. The blue, green and red lines from top to bottom, respectively, correspond to the results with $g_{BL} = g_{BL}|_{max} = 0.727$, 0.6 and $g_{BL}|_{min} = 0.431$ (see Table II).

Using this in Eq. (30), we numerically solve the Boltzmann equation of Eq. (28) and then evaluate the DM relic density by Eq. (31). In Fig. 4, we show the resultant DM relic densities as a function of m_{DM} . The left panel shows $\Omega_{DM}h^2$ for $a = 0.5$ (blue line), $a = 1$ (green line) and $a = 2$ (red line) from top to bottom, respectively, as a function of m_{DM} , along with the observed value (dashed horizontal line) of $\Omega_{DM}h^2 = 0.12$. In this analysis, we have fixed $g_{BL} = 0.6$ and $M_X = 4$ TeV. We see that the observed DM relic density can be reproduced for a suitable choice of $m_{DM} \simeq M_X/2$ for $a \gtrsim 1$. For $a = 1$ and $M_X = 4$ TeV, we show the resultant $\Omega_{DM}h^2$ in the right panel. The blue, green and red lines from top to bottom, respectively, correspond to the results with $g_{BL} = g_{BL}|_{max} = 0.727$, 0.6 and $g_{BL}|_{min} = 0.431$ (see Table II). Our results indicate that an enhancement of the DM annihilation cross section by the X boson resonance effect is crucial for reproducing the observed DM relic density. We have checked that for the parameters used in this analysis, the annihilation cross section of the process (ii) is negligibly small compared with the process (i).

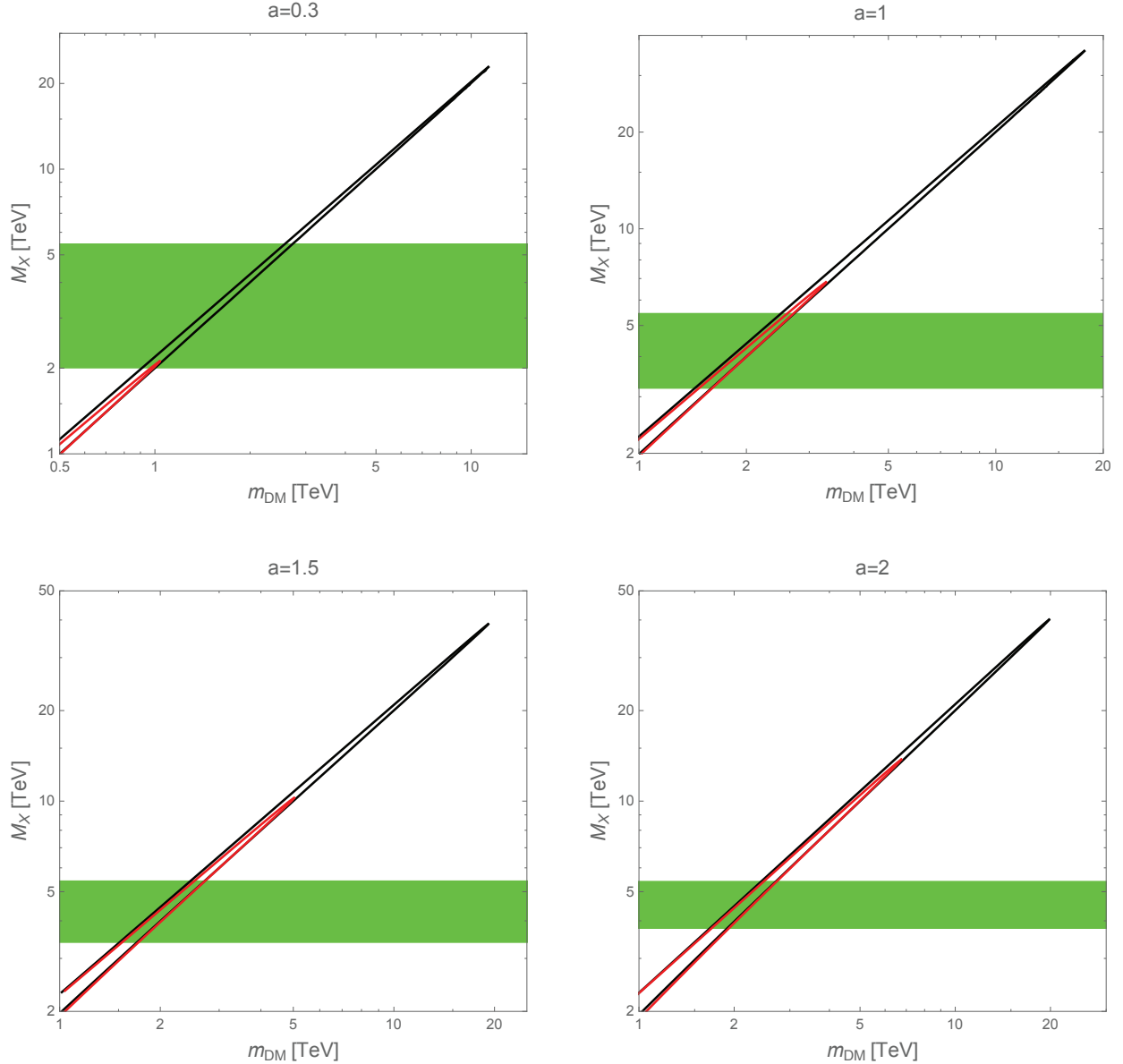


FIG. 5. The parameter region to reproduce the observed DM relic density for various a values. The black and red solid lines correspond to the results for $g_{BL}|_{min}$ and $g_{BL}|_{max}$, respectively, along which $\Omega_{DM}h^2 = 0.12$ is reproduced. The green shaded regions depict the ranges of M_X which simultaneously satisfy the perturbativity condition and the LHC Run-2 constraints.

As can be seen from Fig. 4, for fixed values of a , g_{BL} and M_X , the DM mass to reproduce the observed DM relic density is read off from an intersection of the solid line and the dashed line. In Fig. 5, we show the relations between m_{DM} and M_X for $a = 0.3, 1, 1.5$ and 2 , respectively, so as to reproduce the observed DM relic density. In each panel, the black and red solid lines correspond to the results for $g_{BL}|_{min}$ and $g_{BL}|_{max}$, respectively, along which

$\Omega_{DM}h^2 = 0.12$. The green shaded regions depict the ranges of M_X which simultaneously satisfy the perturbativity condition and the LHC Run-2 constraints (see the right panel of Fig. 3). Now we can see that the allowed parameter region is very limited after combining all the constraints.

Next we consider the case that the process (ii) $\zeta_\ell \zeta_\ell \rightarrow X X$ dominates the annihilation cross section. We can see from Fig. 4, the cross section of the process (i) sharply drops as m_{DM} goes away from the X boson resonance point. For $m_{DM} > M_X$, the process (ii) can dominate the annihilation cross section if g_ζ is sufficiently large.

Since the process (ii) is an s -wave annihilation process, we approximate the thermal averaged cross section in the non-relativistic limit by

$$\langle \sigma v_{rel} \rangle \simeq \sigma v_{rel} \simeq \frac{g_\zeta^4}{16\pi m_{DM}^2} \left(1 - \frac{M_X^2}{m_{DM}^2}\right)^{3/2} \left(1 - \frac{M_X^2}{2m_{DM}^2}\right)^{-2}. \quad (33)$$

With this formula, we solve the Boltzmann equations. For the s -wave annihilation process, the asymptotic solution of the Boltzmann equation is known, and the relic DM density is approximately given by [35, 36]

$$\Omega_{DM}h^2 \simeq \frac{2.13 \times 10^8 x_f}{\sqrt{g_*} M_P \langle \sigma v_{rel} \rangle}, \quad (34)$$

where $x_f = m_{DM}/T_f \simeq \ln(x) - 0.5 \ln(\ln(x))$ with $x = 0.19 \sqrt{g_{DM}/g_*} M_P m_{DM} \langle \sigma v_{rel} \rangle$ for the freeze-out temperature T_f .

As an example, we set $m_{DM} = 3M_X$ in our analysis. We find that the results for $m_{DM} > M_X$ is almost independent of M_X unless m_{DM} is taken to be close to M_X . We have only two free parameters, g_ζ and m_{DM} , involved in this analysis. The cosmological constraint to reproduce the observed DM density of $\Omega_{DM}h^2 = 0.12$ leads to a relation between g_ζ and $m_{DM} = 3M_X$, which is well approximated by $g_\zeta \simeq 0.506 \sqrt{m_{DM}[\text{TeV}]}$, or equivalently,

$$M_X[\text{TeV}] = \frac{1}{3} \left(\frac{g_\zeta}{0.506} \right)^2. \quad (35)$$

Once a is fixed, M_X is given by a function of g_ζ in the range of $g_\zeta|_{min} \leq g_\zeta \leq g_\zeta|_{max}$. As in Eq. (20), g_f is related to g_ζ through g_{BL} . Therefore, M_X is expressed as a function of g_f in the range of $g_f|_{min} \leq g_f \leq g_f|_{max}$. In Fig. 6, we show this relation for $a = 0.3, 1, 2, 3, 4$ and 5 (black solid curves from left to right), along with the upper bound on g_f from the LHC Run-2 results (diagonal red line). We see that for $M_X \geq 0.25$ TeV, the parameter region to reproduce the observed DM density is excluded by the LHC Run-2 result.

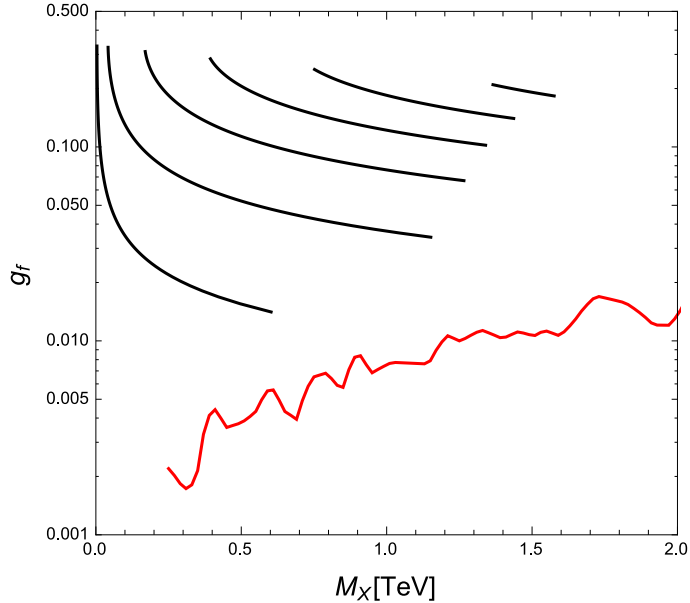


FIG. 6. The plot of M_X versus g_f for the annihilation process (ii) $\bar{\zeta}_\ell \zeta_\ell \rightarrow X X$. The black solid curves from left to right depict the results for $a = 0.3, 1, 2, 3, 4$ and 5 , respectively, from left to right, along which $\Omega_{DM} h^2 = 0.12$ is satisfied. The diagonal red line shows the upper bound on g_f as a function of $M_X \geq 0.25$ TeV from the LHC Run-2 results. No allowed region exists for $M_X \geq 0.25$ TeV, which can simultaneously satisfy the cosmological and LHC constraints.

Before concluding this section, we comment on the DM physics for $|a| \ll 1$. Since $g_\zeta \propto a$, the interaction of the DM particle becomes extremely weak in this case, and the DM particle cannot get in thermal equilibrium with the SM particles. In such a case, we consider the so-called freeze-in DM scenario, in which the DM particles are produced from the annihilations of particles in the thermal plasma. The analysis of our X -portal DM for the freeze-in case is very similar to that in Refs. [38, 39]. Following the analysis in these references, we find that the observed DM density is reproduced for $g_\zeta g_f \sim 10^{-12}$ and $M_X < m_{DM}$, independently of m_{DM} . The condition of $g_\zeta g_f \sim 10^{-12}$ is satisfied by $a \sim 3 \times 10^{-11}$.

VII. CONCLUSIONS

Although the (minimal) left-right symmetric extension of the SM (LRSM) based on the gauge group $\mathcal{G}_{LR} = SU(3)_c \times SU(2)_L \times SU(2)_R \times U(1)_{B-L}$ is a well-motivated direction to new physics beyond the SM, a candidate of the DM particle in our universe is missing. To supplement the LRSM with a suitable DM candidate, we have proposed a minimal extension

of the LRSM by introducing a new $U(1)_X$ gauge interaction along with a vector-like fermions $\zeta_{L,R}$ and a Higgs boson ϕ_X which are singlet under $SU(3)_c \times SU(2)_L \times SU(2)_R$. Through the spontaneous braking of the gauge symmetry $\mathcal{G}_{LR} \times U(1)_X$ down to the SM ones, we obtain the extra gauge boson mass eigenstates, W_R , Z_R and X , and at the same time a Majorana masses for $\zeta_{L,R}$ are generated. The lightest Majorana mass eigenstate ζ_ℓ (whose left-handed component is) defined as a liner combination of ζ_L and ζ_R^c is stable due to the $U(1)_X$ symmetry and hence the DM candidate in our model. For simplicity, we have set the breaking scale of the $SU(2)_R \times U(1)_{B-L}$ to be $v_R = 100$ TeV, and focused on X -portal DM physics. We have considered a variety of phenomenological constraints on this DM scenario to identify the allowed parameter region.

Corresponding to the gauge groups $SU(2)_R$, $U(1)_{B-L}$ and $U(1)_X$, three new gauge couplings, g_R , g_{BL} and g_X , are involved in our model. Imposing the $L \leftrightarrow R$ symmetry, we set $g_R = g$. To reproduce the SM hypercharge gauge coupling, g_X (g_{BL}) is given as a function of g_{BL} (g_X) and a (the $U(1)_X$ charge of ϕ_X). We have derived the interactions of the X boson with the SM fermions and the Majorana fermion DM ζ_ℓ and obtained the expression of the corresponding gauge couplings g_f and g_ζ as a function of only two free parameters, g_{BL} and a . Employing the RG equations at the one-loop level, we have examined the perturbativity condition on the gauge couplings, $g_{BL}, g_X \leq 4\pi$, up to the (reduced) Planck scale and found that the gauge couplings at v_R are constrained to be within certain ranges, $g_{BL}|_{min} \leq g_{BL} \leq g_{BL}|_{max}$ and $g_X|_{min} \leq g_X \leq g_X|_{max}$, once a is fixed. The value of a is also constrained to satisfy $|a| \leq 5.28$. Correspondingly, g_f and g_ζ are constrained to be certain ranges for a fixed a values.

If kinematically allowed, the X boson can be produced at the LHC. The ATLAS and the CMS collaborations have reported their final LHC Run-2 results on the search for a narrow resonance with dilepton final states. Calculating the dilepton production cross section through the X boson resonance in our model, we have interpreted the LHC Run-2 results into the upper bound on g_f as a function of $0.25 \leq M_X[\text{TeV}] \leq 6$. Combining this LHC constraint with the result obtained from the perturbativity condition, we have identified a range of M_X for a fixed a value.

Finally, we have investigated the DM physics. The DM particle ζ_ℓ communicates with the SM particles (fermions) through the interaction with the X boson. In the early universe, the DM particle was in thermal equilibrium with the SM particles, and the DM relic density

at present is evaluated by solving the Boltzmann equation. We have considered two main processes for the DM pair annihilations: (i) $\zeta_\ell \zeta_\ell \rightarrow X \rightarrow f_{SM} \overline{f_{SM}}$ and (ii) $\zeta_\ell \zeta_\ell \rightarrow X X$. The process (i) dominates for $m_{DM} \simeq M_X/2$ while the process (ii) dominates for $m_{DM} > M_X$. Applying the cosmological constraint, $\Omega_{DM} h^2 = 0.12$, we have identified the allowed parameter region for the process (i). Combining the results with the perturbative condition and the LHC Run-2 constraints, we have found the allowed parameter region to be very narrow. As for the process (ii), we have found that the parameter region (g_f as a function of M_X) satisfying the cosmological constraint appears far above the upper bound on g_f (for $M_X \geq 0.25$ TeV), and no allowed parameter region exists.

From Fig. 5, we can see that a suitable choice of $m_{DM} \simeq M_X/2$ can reproduce the observed DM density for a wide range of M_X value while the severe constraints are from the combination of the LHC results and the perturbativity condition. The narrow resonance search at the LHC will continue with the High-Luminosity upgrade of the LHC (HL-LHC). In the X boson search with dilepton final states for $M_X > 1$ TeV, the number of the SM background events is very small, and we expect that the upper bound on $\sigma(pp \rightarrow X \rightarrow \ell^+ \ell^-)$ will be scaled by $1/\mathcal{L}$ with the LHC integrated luminosity \mathcal{L} . Since $\sigma(pp \rightarrow X \rightarrow \ell^+ \ell^-) \propto g_f^2$ in the narrow decay width approximation, our naive prospect for the HL-LHC experiments with the goal integrated luminosity of $\mathcal{L} = 3000/\text{fb}$ is that the current upper bound on g_f shown in the left panel of Fig. 3 will be improved by a factor $\sqrt{139/3000} \sim 0.2$. Therefore, a significant portion of the allowed parameter region presented in this paper will be tested at the HL-LHC experiments.

ACKNOWLEDGEMENT

M. J. Neves would like to thank the Department of Physics & Astronomy at the University of Alabama for the hospitality during his visit as a J-1 Research Scholar. This work is supported in part by the Conselho Nacional de Desenvolvimento Científico e Tecnológico (CNPq) under grant 313467/2018-8 (GM) (M. J. Neves), the United States Department of Energy grant DE-SC0012447 (N. Okada), and the M. Hildred Blewett Fellowship of the

- [1] J. C. Pati and A. Salam, “Lepton Number as the Fourth Color,” *Phys. Rev. D* **10**, 275-289 (1974) [erratum: *Phys. Rev. D* **11**, 703-703 (1975)]
- [2] R. N. Mohapatra and J. C. Pati, “A Natural Left-Right Symmetry,” *Phys. Rev. D* **11**, 2558 (1975)
- [3] G. Senjanovic and R. N. Mohapatra, “Exact Left-Right Symmetry and Spontaneous Violation of Parity,” *Phys. Rev. D* **12**, 1502 (1975)
- [4] P. Minkowski, “ $\mu \rightarrow e\gamma$ at a Rate of One Out of 10^9 Muon Decays?,” *Phys. Lett.* **67B**, 421 (1977).
- [5] T. Yanagida, “Horizontal Symmetry and Masses of Neutrinos,” *Prog. Theor. Phys.* **64**, 1103 (1980); T. Yanagida, in *Proceedings of the Workshop on the Unified Theory and the Baryon Number in the Universe* (O. Sawada and A. Sugamoto, eds.), KEK, Tsukuba, Japan, 1979, p. 95.
- [6] M. Gell-Mann, P. Ramond, and R. Slansky, *Supergravity* (P. van Nieuwenhuizen et al. eds.), North Holland, Amsterdam, 1979, p. 315;
- [7] S. L. Glashow, The future of elementary particle physics, in *Proceedings of the 1979 Cargèse Summer Institute on Quarks and Leptons* (M. Levy et al. eds.), Plenum Press, New York, 1980, p. 687.
- [8] R. N. Mohapatra and G. Senjanovic, “Neutrino Mass and Spontaneous Parity Violation,” *Phys. Rev. Lett.* **44**, 912 (1980).
- [9] A. M. Sirunyan *et al.* [CMS], “Search for a heavy right-handed W boson and a heavy neutrino in events with two same-flavor leptons and two jets at $\sqrt{s} = 13$ TeV,” *JHEP* **05**, 148 (2018) [arXiv:1803.11116 [hep-ex]].
- [10] M. Aaboud *et al.* [ATLAS], “Search for $W' \rightarrow tb$ decays in the hadronic final state using pp collisions at $\sqrt{s} = 13$ TeV with the ATLAS detector,” *Phys. Lett. B* **781**, 327-348 (2018) [arXiv:1801.07893 [hep-ex]].
- [11] A. Maiezza, M. Nemevsek, F. Nesti and G. Senjanovic, “Left-Right Symmetry at LHC,” *Phys. Rev. D* **82**, 055022 (2010) [arXiv:1005.5160 [hep-ph]].

- [12] Y. Mambrini, N. Nagata, K. A. Olive, J. Quevillon and J. Zheng, “Dark matter and gauge coupling unification in nonsupersymmetric SO(10) grand unified models,” *Phys. Rev. D* **91**, no.9, 095010 (2015) [arXiv:1502.06929 [hep-ph]].
- [13] J. Heeck and S. Patra, “Minimal Left-Right Symmetric Dark Matter,” *Phys. Rev. Lett.* **115**, no.12, 121804 (2015) [arXiv:1507.01584 [hep-ph]].
- [14] T. Bandyopadhyay and A. Raychaudhuri, “Left–right model with TeV fermionic dark matter and unification,” *Phys. Lett. B* **771**, 206-212 (2017) [arXiv:1703.08125 [hep-ph]].
- [15] C. Garcia-Cely and J. Heeck, “Phenomenology of left-right symmetric dark matter,” *JCAP* **03**, 021 (2016) [arXiv:1512.03332 [hep-ph]].
- [16] A. Berlin, P. J. Fox, D. Hooper and G. Mohlabeng, “Mixed Dark Matter in Left-Right Symmetric Models,” *JCAP* **06**, 016 (2016) [arXiv:1604.06100 [hep-ph]].
- [17] S. Patra, “Dark matter, lepton and baryon number, and left-right symmetric theories,” *Phys. Rev. D* **93**, no.9, 093001 (2016) [arXiv:1512.04739 [hep-ph]].
- [18] D. Borah, A. Dasgupta, U. K. Dey, S. Patra and G. Tomar, “Multi-component Fermionic Dark Matter and IceCube PeV scale Neutrinos in Left-Right Model with Gauge Unification,” *JHEP* **09**, 005 (2017) [arXiv:1704.04138 [hep-ph]].
- [19] M. J. Neves, J. A. Helajel-Neto, R. N. Mohapatra and N. Okada, “Minimally Extended Left-Right Symmetric Model for Dark Matter with U(1) Portal,” *JHEP* **12**, 009 (2018) [arXiv:1808.00484 [hep-ph]].
- [20] M. J. Neves and J. A. Helajel-Neto, “TeV- and MeV-physics out of an $SU_L(2) \times U_R(1)_J \times U(1)_K$ model,” *Annalen Phys.* **530**, no.3, 1700112 (2018) [arXiv:1609.08471 [hep-ph]].
- [21] S. Okada, “ Z' Portal Dark Matter in the Minimal $B - L$ Model,” *Adv. High Energy Phys.* **2018**, 5340935 (2018) [arXiv:1803.06793 [hep-ph]].
- [22] R. N. Mohapatra and G. Senjanovic, “Neutrino Masses and Mixings in Gauge Models with Spontaneous Parity Violation,” *Phys. Rev. D* **23**, 165 (1981)
- [23] J. F. Gunion, J. Grifols, A. Mendez, B. Kayser and F. I. Olness, “Higgs Bosons in Left-Right Symmetric Models,” *Phys. Rev. D* **40**, 1546 (1989)
- [24] G. Barenboim, M. Gorbahn, U. Nierste and M. Raidal, “Higgs Sector of the Minimal Left-Right Symmetric Model,” *Phys. Rev. D* **65**, 095003 (2002) [arXiv:hep-ph/0107121 [hep-ph]].
- [25] K. Kiers, M. Assis and A. A. Petrov, “Higgs sector of the left-right model with explicit CP violation,” *Phys. Rev. D* **71**, 115015 (2005) [arXiv:hep-ph/0503115 [hep-ph]].

- [26] P. S. B. Dev, R. N. Mohapatra and Y. Zhang, “Probing the Higgs Sector of the Minimal Left-Right Symmetric Model at Future Hadron Colliders,” *JHEP* **05**, 174 (2016) [arXiv:1602.05947 [hep-ph]].
- [27] A. Maiezza, M. Nemevšek and F. Nesti, “Perturbativity and mass scales in the minimal left-right symmetric model,” *Phys. Rev. D* **94**, no.3, 035008 (2016) [arXiv:1603.00360 [hep-ph]].
- [28] M. Nemevšek, F. Nesti and J. C. Vasquez, “Majorana Higgses at colliders,” *JHEP* **04**, 114 (2017) [arXiv:1612.06840 [hep-ph]].
- [29] A. Maiezza, G. Senjanović and J. C. Vasquez, “Higgs sector of the minimal left-right symmetric theory,” *Phys. Rev. D* **95**, no.9, 095004 (2017) [arXiv:1612.09146 [hep-ph]].
- [30] P. S. Bhupal Dev, R. N. Mohapatra, W. Rodejohann and X. J. Xu, “Vacuum structure of the left-right symmetric model,” *JHEP* **02**, 154 (2019) [arXiv:1811.06869 [hep-ph]].
- [31] G. Aad *et al.* [ATLAS], “Search for high-mass dilepton resonances using 139 fb^{-1} of pp collision data collected at $\sqrt{s} = 13 \text{ TeV}$ with the ATLAS detector,” *Phys. Lett. B* **796**, 68-87 (2019) [arXiv:1903.06248 [hep-ex]].
- [32] CMS Collaboration, “Search for a narrow resonance in high-mass dilepton final states in proton-proton collisions using 140 fb^{-1} of data at $\sqrt{s} = 13 \text{ TeV}$,” CMS-PAS-EXO-19-019.
- [33] J. Pumplin, D. R. Stump, J. Huston, H. L. Lai, P. M. Nadolsky and W. K. Tung, “New generation of parton distributions with uncertainties from global QCD analysis,” *JHEP* **07**, 012 (2002) [arXiv:hep-ph/0201195 [hep-ph]].
- [34] N. Aghanim *et al.* [Planck], “Planck 2018 results. VI. Cosmological parameters,” *Astron. Astrophys.* **641**, A6 (2020) [arXiv:1807.06209 [astro-ph.CO]].
- [35] E. W. Kolb and M. S. Turner, “The Early Universe,” *Front. Phys.* **69**, 1-547 (1990)
- [36] G. Bertone, D. Hooper and J. Silk, “Particle dark matter: Evidence, candidates and constraints,” *Phys. Rept.* **405**, 279-390 (2005) [arXiv:hep-ph/0404175 [hep-ph]].
- [37] N. Aghanim *et al.* [Planck Collaboration], *Planck 2018 results. VI. Cosmological parameters*, *A & A* **641**, A6 (2020) [arXiv:astro-ph.CO/1807.06209v3].
- [38] R. N. Mohapatra and N. Okada, “Dark Matter Constraints on Low Mass and Weakly Coupled B-L Gauge Boson,” *Phys. Rev. D* **102**, no.3, 035028 (2020) [arXiv:1908.11325 [hep-ph]].
- [39] N. Okada, S. Okada and Q. Shafi, “Light Z' and dark matter from $U(1)_X$ gauge symmetry,” *Phys. Lett. B* **810**, 135845 (2020) [arXiv:2003.02667 [hep-ph]].